Electrode potential from density functional theory calculations combined with implicit solvation theory

Jun Haruyama,* Tamio Ikeshoji, and Minoru Otani*
Research Center for Computational Design of Advanced Functional Materials (CD-FMat), National Institute of Advanced Industrial Science and Technology (AIST), 1-1-1 Umezono, Tsukuba, Ibaraki 305-8568, Japan

(Received 17 June 2018; revised manuscript received 3 August 2018; published 13 September 2018)

We present a method that makes it possible to determine an electrode potential in an electrode/electrolyte solution system. We consider the electrode potential of the standard hydrogen electrode (SHE) reaction R : $1/2\,H_2(\mathrm{gas}) + H_2O\,(1\,\mathrm{M\,HCl\,aq.}) \leftrightarrow H_3O^+(1\,\mathrm{M\,HCl\,aq.}) + e^-$ (electrode M), and conduct density functional theory (DFT) calculations combined with the effective screening medium (ESM) method and the reference interaction site model (RISM). The electrostatic field from a charged slab described by DFT with ESM is screened by that from the charge distribution in an electrolyte solution. This screening enables us to define the inner potential Φ_S at the bulk solution region, which is the reference potential for the electrode potential, that is, the chemical potential of electrons (μ_e). Grand potentials of the left and right sides in reaction R at the equilibrium point derive the corresponding SHE potential of $\mu_e^{\mathrm{SHE}} = -5.27\,\mathrm{eV}$ vs Φ_S for a Pt(111) electrode. Another pathway that uses the free energy difference gives the same SHE potential; the equivalence of the electrode potentials from chemical potential and from free energy difference is validated within ESM-RISM. Even using a different electrode of Al yields the value of $\mu_e^{\mathrm{SHE}} = -5.22\,\mathrm{eV}$ vs Φ_S, which indicates that the electrode potential is independent of the electrodes. Finally, the potential energy profile in a vacuum/metal/solution/vacuum region shows that a difference between the inner and outer potentials is necessary to compare an absolute SHE potential and the SHE potential vs Φ_S.

DOI: 10.1103/PhysRevMaterials.2.095801

I. INTRODUCTION

Electrochemical energy conversion and storage have become a requisite technology owing to the continuously expanding demand from mobile phones and electric vehicles in the last few decades. An interface between a metal electrode and an electrolyte solution has attracted much scientific and engineering attention for a long time [1]. To manage, control, and suppress the rate-determining and energy-loss processes occurring at the electrode/solution interface, a basic understanding of elementary charge-transfer reactions at the molecular level is crucial to achieve highly efficient electrochemical devices such as fuel cells [2] and innovative secondary batteries [3].

To consider electrochemical reactions at the interface, the electrode potential is a general concept as it governs charge transfer (CT) reactions such as the oxygen reduction, hydrogen evolution, and ion insertion/extraction processes. Therefore, to simulate the CT reactions at the molecular level, the electrode potential must be correctly defined (or precisely included) in a microscopic model. In experiments, half-cell electrode potentials are given relative to a chosen reference electrode for electrochemically stable reactions, for example, standard hydrogen electrode (SHE), reversible hydrogen electrode (RHE), saturated calomel electrode (SCE), silver/silver chloride electrode (Ag/AgCl), and lithium metal electrode (Li^+/Li). Especially, the SHE potential, which is the equilibrium potential of the H^+/H_2 charge transfer reaction under standard conditions, that is, $p\mathrm{H} = 0$ (or $1\,\mathrm{M\,H^+}$) aqueous solution, pressure of 1 bar, and temperature of 298.15 K, is recommended as the reference potential of electrochemical reactions.

In many electrochemical experiments, taking the potential difference between two electrodes is sufficient to compare the electrochemical measurements. However, an absolute potential scale is necessary when comparing electrochemical measurements with physical observations of photo- and electron-induced spectra, especially work functions [4]. A lot of research has been conducted to obtain the absolute SHE potential $E(H^+/H_2)$ [abs], which is defined as the SHE potential with respect to a universal reference system (without any additional electrode/solution interface). According to Trasatti, the absolute electrode potential corresponds to the "work functions" of metals in solution [5]. Because of the difficulty arising from the determination of work functions, the values that have been reported by several groups cover a large range ($4.28 \leqq E(H^+/H_2)\,[\mathrm{abs}] \leqq 4.85\,\mathrm{V}$) [6].

In 1986, Trasatti suggested two different ways to measure $E(H^+/H_2)$ [abs] and obtained almost the same value [7]. One way is to apply the following Born-Haber cycle to the charge transfer reaction of H^+/H_2:

$$\begin{array}{ccc} \mathrm{H(gas)} & \xrightarrow{\Delta_{\mathrm{ion}}G^\circ} & \mathrm{H^+(gas) + e^-(vac.)} \\ \uparrow \Delta_{\mathrm{at}}G^\circ & & \downarrow \alpha_{\mathrm{H^+}}^{\circ,\mathrm{S}} \quad \downarrow \mu_e \\ \mathrm{1/2\,H_2(gas)} & \xrightarrow[-\Delta G_{\mathrm{SHE}}]{} & \mathrm{H^+(S) + e^-(M)} \end{array}, \qquad (1)$$

*Corresponding authors: haruyama-jun@aist.go.jp; minoru.otani@aist.go.jp

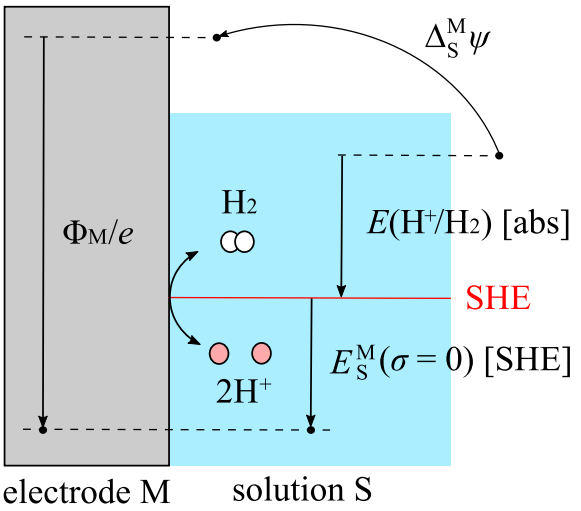

FIG. 1. Schematic potential path for the calculation of the absolute SHE potential.

where $\Delta_{at}G^\circ$ and $\Delta_{ion}G^\circ$ are the (standard) atomization and ionization Gibbs free energies of H_2 and H, respectively. The (standard) real solvation Gibbs free energy of H^+ in the solution S is represented as $\alpha^{\circ,S}_{H^+}$, which is the necessary work to bring H^+ in gas to the solution and includes the surface potential contribution. While we use the expression of $\alpha^{\circ,S}_{H^+}$ for the real free energy of solvation, which can be measured, we use the expression of ΔG_{solv} for the conventional free energy of solvation, which does not include the surface potential contribution. If we define the chemical potential of electrons as $\mu_e = 0$, the free energy difference of reaction H^+/H_2, defined as ΔG_{SHE}, gives the absolute SHE potential as

$$E(H^+/H_2)[\text{abs}] = -\Delta G_{SHE}/F = (\Delta_{at}G^\circ + \Delta_{ion}G^\circ + a^{\circ,S}_{H^+})/F, \quad (2)$$

where F is the Faraday constant, and Eq. (2) contains mainly thermodynamic quantities. Since the free energies of H_2(gas) and H^+(S) are independent of the electrode M, on the condition that H^+ is solvated in the bulk without any influence from electrode M, the equilibrium of the reaction H^+/H_2 uniquely determines the electrode potential and the corresponding μ_e. Another way is derived from the potential path, as shown in Fig. 1. The absolute SHE potential is represented by the work function of the metal electrode Φ_M, contact (or Volta) potential difference $\Delta_S^M\psi$, and the potential of zero charge (PZC) of the metal electrode M measured from the SHE reference $E_S^M(\sigma = 0)$ [SHE]:

$$E(H^+/H_2)[\text{abs}] = \Phi_M/e + \Delta_S^M\psi - E_S^M(\sigma = 0)[\text{SHE}], \quad (3)$$

where e and σ are the elementary charge and the surface charge density, respectively. Equation (3) contains the physical quantity of Φ_M/e and the electrochemical measurements of $\Delta_S^M\psi$ and $E_S^M(\sigma = 0)$ [SHE]. Trasatti chose the electrode M = Hg and obtained the same value of 4.44 V as that obtained from Eq. (2), and this value is recommended by the International Union of Pure and Applied Chemistry (IUPAC) [8].

From the standpoint of density functional theory (DFT) based molecular dynamics (MD) studies, the calculation method for $\Delta_S^M\psi$ and $E_S^M(\sigma = 0)$ has been gradually improved during the past decade. While specific adsorptions of electrolyte ions cause experimental difficulty for determining these values, it is possible to calculate these values for clean metal surfaces by DFT. In the seminal study by Otani *et al.* in 2008 [9], they developed an approach using a novel computational scheme called an effective screening medium (ESM). This method can incorporate an open boundary condition (OBC) for the Poisson equation in the surface normal direction. They showed that the OBC-applied DFT-MD configurations gave the contact potential difference $\Delta_S^M\psi$ measured in experiments. Water and the interface structures on the Pt electrode have been studied from various aspects by applying the ESM technique [10].

Subsequent studies have been reported by various groups. Tripkovic *et al.* applied static water adsorption structures on the electrode [11], and Sakong *et al.* performed periodic boundary condition (PBC) based dispersion corrected DFT-MD calculations [12]. They employed a work function method in which a water-vapor interface was explicitly modeled and the vacuum potential was chosen as a reference. An alternative SHE computation method [13] developed by Cheng and Sprik avoided treating the water-vapor interface and referred to the solvation free energy of H^+(S), which was calculated using a thermodynamic integration technique [14], and allowed for the direct estimation of $E_S^M(\sigma = 0)$ [SHE]. The recently developed computational SHE method by Le *et al.* in 2017 enabled calculation of $E_S^M(\sigma = 0)$ [SHE] of metal electrodes at an affordable cost [15]. DFT-MD simulations have enabled the estimation of the electrochemical measurements of $\Delta_S^M\psi$ and $E_S^M(\sigma = 0)$ with good accuracy; however, microscopic calculations when the electrode potential is shifted from PZC (in $\sigma \neq 0$) is still a challenging task.

Nørskov *et al.* proposed the computational hydrogen electrode (CHE) model, which allows for the estimation of the free energy of intermediates, as a function of the electrode potential, by DFT calculations of the surface adsorption energies [16]. The CHE analysis can explain the volcano-shaped relationship between the cathode reaction rate and the oxygen adsorption energy [17]. By setting the reference potential to be that of the SHE, the CHE is able to obtain the chemical potential for the reaction $(H^+ + e^-)$ as that of $H_2/2$. The effect of a bias on all states involving an electron in the electrode is indirectly included by shifting the energy of this state by $-eE$ [SHE], where E [SHE] is the *hypothetical electrode potential*. The effect of the electric field on the adsorption energy is assumed to be small [18]. Surface Pourbaix diagrams can also be obtained by employing the CHE concept [19].

The CHE model is a practical way to explore reaction energetics without explicit treatment of electrons and ions in solution. However, it is necessary to include the solvent, excess charge, and electrode potential in the model system when analyzing charge transfer kinetics barriers [20–22]. Many schemes have been proposed to treat charged electrochemical interfaces [23–29]. The electrode in one of these schemes is immersed in an homogeneous background charge

and the electrode potential is treated using the double-reference method [23]. The electrodes in other schemes interact with an implicit solvent, which is represented by modified Poisson-Boltzmann (MPB) equations [24], the joint density-functional theory (JDFT) [25], the polarizable continuum model (PCM) [26,27], and the singlet reference interaction site model (SRISM) [28,29].

The crucial property required in an electrochemical interface system (and computing electrode potential) is the grand canonical condition for electrons in the electrode as well as solvent molecules and electrolyte ions in the solution; the numbers of electrons N_e and electrolyte ions should change in a calculation cell. Instead of a free energy, a *grand potential* Ω is a precise quantity to describe the behavior of the system [30–32]. As discussed by Lozovoi *et al.* [31], a calculation with the condition of a constant N_e resembles an isolated system such as a disconnected capacitor. A system with constant μ_e, however, corresponds to metallic slabs in an electric circuit where the voltage between the focusing electrode and counter (or referenced) electrode is controllable.

By introducing an extended system as a reservoir of electrons, a potentiostat scheme that realizes the constant-μ_e condition for performing DFT-MD simulation with ESM was developed by Bonnet *et al.* [32]. The number of cation and anion in the electrolyte should be changed to compensate for the excess electrons in the electrochemical half-cell. Thus, the microscopic simulations under the constant-μ_e condition are regarded as constant-potential measurements in electrochemistry. The chemical potential of electrons μ_e is a control variable to cause electrochemical reactions, and it is identical to the electrode potential E. However, a conversion relationship between μ_e and E is necessary to compare simulation results with experiments.

In this study, DFT calculations combined with the ESM technique and the reference interaction site model (RISM), termed as ESM-RISM, were applied to the electrode/solution interfaces. This is an electronic structure calculation that includes additional self-consistent interactions with implicit solvent molecules and ions in solution, which is similar to the QM/MM (the quantum mechanics and molecular mechanics) method. The ESM-RISM formulation is able to realize the grand canonical condition for not only electrons but also the RISM components in the solution; the electron density is calculated as the sum of Kohn-Sham orbitals up to a given μ_e, and the excess charge is compensated for by the charge difference in the electrolyte in the solution represented by RISM. An electric double layer is spontaneously formed at the electrode/solution interface, and the charge neutrality in the total system is always satisfied. These grand canonical properties give a well-defined inner potential Φ_S at the bulk solution region. The objective of this study is to obtain μ_e, corresponding to the SHE potential μ_e^{SHE} measured from Φ_S, by applying the grand potential analysis based on the ESM-RISM calculation.

This article is organized as follows. Section II describes the ESM-RISM formulation, the inner potential in ESM-RISM calculations, electrode potentials from thermodynamic and electrochemical relations, and the computational details. Section III provides grand potentials as a function of the chemical potential of electrons on Pt(111) and Al(111) electrodes. The equivalence between the electrode potentials from chemical potential and from free energy difference is also discussed. The potential profile at the interface of vacuum/metal/solution/vacuum is presented in Sec. IV, which indicates the relationship between the SHE potential measured from the inner potential and the absolute SHE potential. Finally, Sec. V gives the conclusions of this study.

II. METHODS, MODELS, AND CONCEPTS

A. ESM-RISM

In this subsection we briefly describe the ESM-RISM formulation. Since the number of electrons is variable in an electrochemical charge-transfer system, we first define the grand potential Ω:

$$\Omega \equiv A - \mu_e\left(N_e - N_e^0\right) = A - \mu_e \Delta N_e, \tag{4}$$

where the Helmholtz free energy A, the chemical potential of electrons μ_e, and the number of electrons N_e are introduced. The Ω of Eq. (4) is changed by the number of electrons, where the difference ΔN_e from that at a charge neutral electrode (N_e^0) is used. Therefore, the $-\Delta N_e$ refers the number of excluded electrons from the electrode under the external condition of μ_e. In the expression of Eq. (4), the chemical potential contributions from particles other than electrons are omitted. Because the RISM formulation treats only the excess free energy, as explained below, it is not necessary to consider chemical potential contributions from RISM particles. ESM-RISM describes the Helmholtz free energy A as

$$A = E_{DFT} + \Delta A_{RISM}, \tag{5}$$

where E_{DFT} is the DFT total energy derived from the Kohn-Sham (KS) equation [33]. When we consider the reaction including the change of hydrogen-related bond, we should include zero point energy in E_{DFT}. In addition, E_{DFT} is approximately used instead of the free energy. The difference is generally small, but entropy terms should be considered in some cases such as gas phase reactions. An additional self-consistent potential arising from the interaction between electrons and RISM solvents is considered in solving the KS equation, which is referred to as the solvent potential v_{solv}. This description was developed by Kovalenko and Hirata [34]. The excess free energy resulting from interactions between QM particles and the RISM solvents is expressed as ΔA_{RISM}. The self-consistent KS orbitals and the distribution functions of RISM components are determined with the ESM open boundary condition and derived from Laue-represented RISM equations, respectively [35,36]. The interactions between QM ions (nucleus) and the reference sites are represented by Coulomb and Lennard-Jones (LJ) potentials. The solvation structure arising from implicit solvent is automatically distributed around the explicit molecules, ions, and a metal surface once the RISM equation is solved. The system-specific parameters which combine DFT with implicit solvent are LJ parameters of the explicit atoms. The same potential forms are used between the reference sites. It is worth mentioned that the accuracy of solvation effects depends on the LJ parameters and effective charges, that is, force-field parameters.

In this study, ESM-RISM calculations were performed on the configuration of a vacuum/slab/solvent,

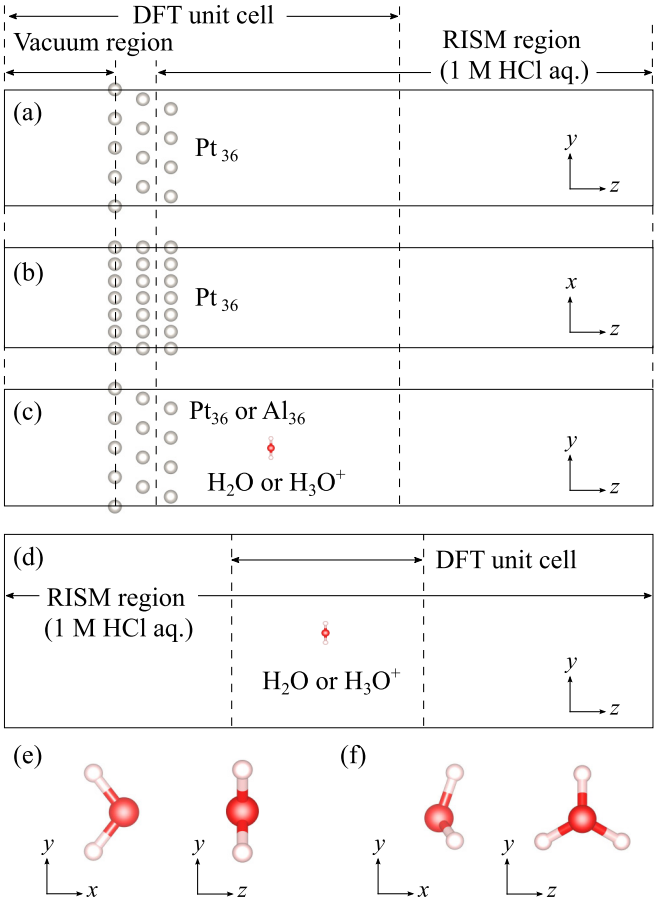

FIG. 2. Settings of ESM-RISM calculation: (a) and (b) vacuum/slab/solvent, (c) vacuum/slab+ion/solvent, and (d) solvent/ion/solvent systems. The configurations of (e) H_2O and (f) H_3O^+ are also depicted. The Pt, O, and H atoms which are explicitly treated with DFT are shown as gray, red, and white spheres, respectively.

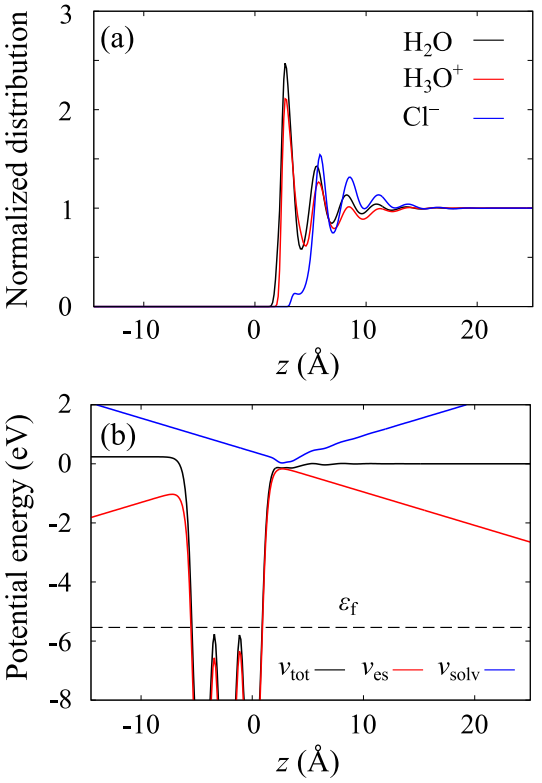

FIG. 3. Planar-average distributions and potential energies on Pt(111)/1 M HCl aq. as a function of the surface-normal coordinate z at $\sigma = -0.125\,e/\mathrm{nm}^2$. (a) The distributions of H_2O, H_3O^+, and Cl^- solvents are represented by the black, red, and blue lines, respectively. (b) The total potential v_{tot}, electrostatic potential v_{es}, and solvent potential v_{solv} are represented by the black, red, and blue lines, respectively. The Fermi level ε_{f} is depicted as a dashed line.

vacuum/slab+ion/solvent, and solvent/ion/solvent systems, as shown in Fig. 2. The slabs consisted of metal atoms, and the solvent included dissolved electrolytes. In the vacuum/slab/solvent system in Figs. 2(a) and 2(b), the slab domain of Pt(111) was treated by DFT + ESM and the aqueous solution of hydrochloric acid (HCl aq.) in the solvent was treated by RISM. As the solute and solvent are not distinguished in RISM, a mixture of solvent molecules and solute ions is called the "solvent." The solvent condition is connected to the concentration of 1 M HCl aq. at the right boundary of the RISM region. The details of the vacuum/slab+ion/solvent and solvent/ion/solvent systems in Figs. 2(c)–2(f) will be presented in Sec. III C.

B. Inner potential

The inner potential (used in this study) is the time and space average electrostatic potential far from interfaces. Since the inner potential should be independent from the interfaces, it can be used as a reference potential. Then, it becomes possible to compare either the free energy A or grand potential Ω with those in other electrochemical systems. In the ESM-RISM calculations, the chemical potential of electrons μ_{e} could be measured from the inner potential Φ_{S} as explained in the following.

The RISM solvent distributions on the Pt(111)/1 M HCl aq. along the surface-normal coordinate were calculated, as shown in Fig. 3(a), where the excess electrons of $-0.1\,e$/unit cell corresponding to a surface charge density $\sigma = -0.125\,e/\mathrm{nm}^2$ were introduced. The normalized distributions of H_2O and H_3O^+ were obtained as the averaged sum of the distribution functions of their constituents (which corresponds to the particle number density of H_2O and H_3O^+, respectively) in the plane parallel to the slab surface. The origin of coordinate z was set at the Pt atoms closest to the solution. The distribution functions exhibited a peak around $z = 3$ Å and decreased in moving towards the bulk with oscillations. Force field parameters used in this RISM calculation were unable to reproduce the specific adsorption behavior of Cl^-, as has been discussed by Luque *et al.* [29]. The analysis of the detailed solution structures is beyond the scope of this study. The solvent distributions almost converged to unity at the over 10 Å region, where the screening distance was consistent with a short Debye length of several angstroms [1] in the concentrated electrolyte solution of 1 M HCl aq.

The total electrostatic potential v_{tot} in the ESM-RISM system consists of two contributions; one is the usual electrostatic potential, which is the sum of the Hartree and ionic core

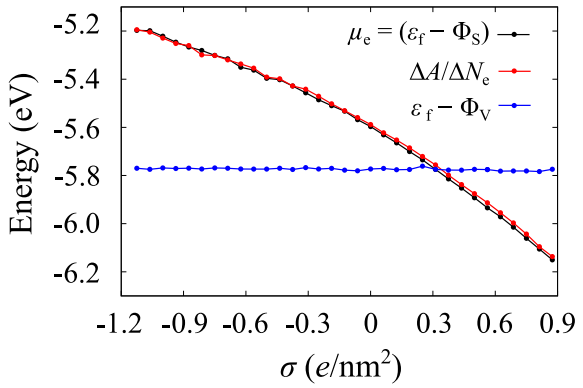

FIG. 4. Chemical potential of electrons μ_e as a function of the surface charge density σ on Pt(111)/1 M HCl aq. The black, red, and blue circles show the calculated values of $\mu_e(=\varepsilon_f - \Phi_S)$, $\Delta A/\Delta N_e$, and $\varepsilon_f - \Phi_V$, respectively.

potentials v_{es}, and the other is the solvent potential, which is described in Sec. II A (v_{solv}) [34]. These three potentials are shown as a function of the z coordinate on Pt(111)/1 M HCl aq. in Fig. 3(b). The Fermi level ε_f of the Pt(111) electrode is also shown in Fig. 3(b). Since the RISM electrolyte screened out the electric field created by the surface charge density, as shown in Fig. 3, the converged potential at the right-hand side is regarded as the inner potential,

$$\Phi_S \equiv \lim_{z \to \infty} v_{tot}(z). \tag{6}$$

The open boundary condition of ESM (based on Green function technique) gives the midpoint of left- and right-side potentials as the zero: $\lim_{z\to\infty}[v_{tot}(z) + v_{tot}(-z)]/2 = 0$ [35]. We shift the energy origin from this zero to the right-side potential, that is, $\Phi_S = 0$. The chemical potential of electrons μ_e is measured from Φ_S.

Since the Fermi level ε_f corresponds to the energy variation by changing the number of electrons in the system, the chemical potential of electrons μ_e [vs Φ_S] satisfies the relation

$$\mu_e[\text{vs } \Phi_S] = \varepsilon_f - \Phi_S = \partial A/\partial N_e. \tag{7}$$

We calculated $\Delta A/\Delta N_e$ numerically as a function of the surface charge density σ on Pt(111)/1 M HCl aq., as shown in Fig. 4. The results showed a good agreement between μ_e [vs Φ_S] and $\Delta A/\Delta N_e$.

When two different electrodes M and M′ are immersed in the same electrolyte solution S, it can be assumed that the two inner potentials Φ_S^M and $\Phi_S^{M'}$ are identical to each other. Thus, the inner potential Φ_S is used as a reference potential in ESM-RISM calculation.

The work function Φ_M of electrode M = Pt(111) is defined as the difference between the potential energy far outside the metal and the Fermi level ε_f of the metal. On the three-layer slab of the Pt(111) surface, $\Phi_M = 5.77$ eV was obtained from conventional DFT calculations. In the ESM-RISM calculation at $\sigma = 0$, the electric double layer polarization at the Pt-solution interface caused a potential energy difference between the left-hand side (vacuum region) $\Phi_V[\equiv \lim_{z\to-\infty} v_{tot}(z)]$ and the right-hand side (solution region) Φ_S, given as $\Phi_S - \Phi_V = -0.17$ eV. As a result, the chemical potential of electrons at PZC ($\sigma = 0$) became $\mu_e^{PZC}(\text{Pt}) = -5.60$ eV vs Φ_S. However, the difference between the Fermi level ε_f and potential energy Φ_V was -5.77 ± 0.01 eV in the region of $-1.2 < \sigma < 0.9\, e/\text{nm}^2$, as shown in Fig. 4. Thus, the opposite sign of $\varepsilon_f - \Phi_V$ in the ESM-RISM calculations was equal to Φ_M regardless of the introduced surface charge density:

$$\Phi_V - \varepsilon_f = \Phi_M \text{ even when } \sigma \neq 0. \tag{8}$$

C. Electrode potential

In this subsection we describe the electric potential of the electrode on which the following SHE charge transfer reaction takes place:

$$1/2\ H_2(\text{gas}) + H_2O(\text{S}) \leftrightarrow H_3O^+(\text{S}) + e^-(\text{M}). \tag{R1}$$

Similar to the two procedures conducted by Trasatti [7], two pathways to evaluate the electrode potential are possible within ESM-RISM calculations using the vacuum/slab+ion/solvent and solvent/ion/solvent systems shown in Figs. 2(c) and 2(d), respectively. The reacting *one* QM molecule/ion (H_2O or H_3O^+) was placed in the solution far from the electrode surface or the center of the simulation cell. The one H_2O molecule/H_3O^+ ion being explicitly treated with DFT is sufficient to describe the electrode potential of H_2/H^+ because the solvation interaction is included in ΔA_{RISM}. The vacuum/slab+ion/solvent and solvent/ion/solvent systems have distinctive characteristics (advantages and drawbacks) in treating the charge transfer reactions.

First, we consider the solvent/ion/solvent system, which treats an isolated ion in a solution phase with no electrode. Owing to the OBC introduced by the ESM technique for the RISM equation, the ESM-RISM calculation of the solvent/ion/solvent system is different from that of the PBC applied 3D-RISM system. The OBC realizes a grand canonical condition for RISM solvents. The inner potential Φ_S in this system is identical to that in the vacuum/slab(+ion)/solvent system. Therefore, an ideal free energy referenced to Φ_S in the solution phase can be obtained from this system, where "ideal" means that the energy arising from interactions between an electrode surface and a reacting ion exactly equals to 0. If the free energies of H_2(gas), H_2O(S), and H_3O^+(S) are calculated from this solvent/ion/solvent system, the electrode potential $E(H^+/H_2)$ referenced to the inner potential Φ_S could be obtained from the free energy difference ΔG_{SHE} without the Born-Haber cycle:

$$E(H^+/H_2)[\text{vs } \Phi_S] = -\Delta G_{SHE}/F[\text{vs } \Phi_S]. \tag{9}$$

The relation in Eq. (9) is almost the same as that in Eq. (2) except for the reference potential. In this study, an electrode potential derived from the ΔG calculation is referred to as the *electrode potential from free energy difference*. Other techniques, such as thermodynamic integration, are also able to access an estimation of the value of ΔG [14,37]. The expression of Eq. (9) formally resembles that of the electromotive force (EMF) $E_{emf} = -\Delta G/nF$, where n is the number of reacted electrons. These free-energy (or thermodynamic) attributed E_{emf} calculations have been widely applied to many kinds of electrode materials, as DFT calculations have given the

experimental Li-intercalation potentials with good accuracy [22,38]. The EMF expression and Eq. (9) are different in terms of the charged and neutral states of their electrochemical reactions. Namely, the former represents a half-cell reaction and the latter represents a full-cell reaction.

The next consideration is the vacuum/slab+ion/solvent system shown in Fig. 2(c). This system mimics realistic electrochemical conditions where a charge transfer reaction occurs. Namely, an ESM-RISM calculation of the vacuum/slab+ion/solvent system treats the interface of the electrode + reacting ion/solution with an explicit inclusion of a chemical potential shift (i.e., a bias potential effect) and influences from double layer structures. The system allows us to calculate Ω at a given μ_e referenced to Φ_S. The equilibrium condition of reaction (R1) is satisfied at μ_e^{SHE}, which corresponds to the SHE potential. As a result, the following simple relation concerning the electrode potential is established:

$$E(H^+/H_2)[\text{vs } \Phi_S] = \mu_e^{SHE}/e[\text{vs } \Phi_S]. \tag{10}$$

We refer to an electrode potential derived from μ_e as the *electrode potential from chemical potential*. Although the electrode potentials from free energy difference and from chemical potential are expressed as different quantities, these two potentials should be equal to each other, as shown by Trasatti [7]. The equivalence of the two electrode potentials is validated within an ESM-RISM treatment, which will be shown in Sec. III.

Once μ_e^{SHE} is determined in the ESM-RISM calculation, any μ_e can be converted to an electrode potential E relative to the SHE potential as

$$E[\text{SHE}] = -\big(\mu_e[\text{vs } \Phi_S] - \mu_e^{SHE}[\text{vs } \Phi_S]\big)/e. \tag{11}$$

To obtain the chemical potential of electrons corresponding to the SHE potential μ_e^{SHE} [vs Φ_S] by applying a constant-μ_e ESM-RISM calculation is the main objective of this study.

D. Computational details

Quantum ESPRESSO code [39] was used to conduct the spin-unpolarized DFT and ESM-RISM calculations. An exchange-correlation functional of the Perdew-Burke-Ernzerhof (PBE) generalized-gradient approximation [40] was adopted with a plane-wave basis within the ultrasoft pseudopotential framework [41]. The electronic configurations were $1s^1$ for H, $2s^2 2p^4$ for O, $3s^2 3p^1$ for Al with nonlinear core correction (NLCC) [42], and $6s^1 6p^0 5d^9$ for Pt with NLCC. The cutoff energies were set to 40 and 320 Ry (1 Ry = 13.606 eV) for the wave functions and the augmented charge, respectively.

Three layer slabs of Pt(111) and Al(111) were constructed by cutting face-centered cubic (fcc) crystals, where the lattice constants were set to 3.924 and 4.049 Å, respectively. The atom positions of Pt and Al were fixed in their crystal positions throughout this study. The simulation cells of Pt(111) and Al(111) of the vacuum/slab(+ion)/solvent systems, shown in Figs. 2(a)–2(c), had a rectangular surface area of 8.324×9.612 Å^2 and 8.590×9.919 Å^2, respectively, with 3×4 atoms per layer. The DFT unit cells had a z-axis length of 40 Å and the RISM region was extended to the right-hand side by 31.875 Å from the DFT region. The vacuum regions were 10 Å. For the solvent/ion/solvent systems, a cubic DFT unit cell of $20 \times 20 \times 20$ Å^3 was adopted and the extended regions of 31.875 Å were added to both sides as the RISM regions, as indicated in Fig. 2(d). Converged k-point sampling of $4 \times 4 \times 1$ was adopted for the vacuum/slab(+ion)/solvent systems. Only the Γ point was chosen for the solvent/ion/solvent system. Electron occupation numbers were determined by the Gaussian smearing technique with a broadening parameter of 0.01 Ry. The atomic positions of H_2O and H_3O^+ in the solvent/ion/solvent system were relaxed until the residual forces became less than 0.001 Ry/bohr (1 bohr = 0.52918 Å), while the atomic positions of H_2O and H_3O^+ in the vacuum/slab+ion/solvent system were fixed at their relaxed configurations of the solvent/ion/solvent system. In the vacuum/slab+ion/solvent system, the distance between O and the right-hand boundary of the DFT cell was set to 15 Å (the distance between O and the first layer Pt or Al surface plane is approximately 10 Å). The VESTA package was used to visualize the coordinates of the DFT atoms in this study [43].

The RISM solvent system consisted of H_2O molecules, with a density of 1.00 g/cm^3(= 55.5 mol/L), and a 1.0 mol/L HCl electrolyte at a temperature of 300 K. The Laue-RISM calculation was performed with the closure of the model by Kovalenko and Hirata [34], and the excess free energy ΔA_{RISM} was evaluated by the Gaussian fluctuation model [44]. The cutoff energy was set to 160 Ry for the distribution functions of the RISM components. The convergence criterion of the correlation functions in the RISM equations was set to 10^{-6} Ry.

The parameters of classical force fields used for RISM calculations were selected from the literature as follows. The simple point charge (SPC) [45] and TIP5P [46] models were tested for an H_2O molecule with modifications of some LJ parameters. We took the parameters by Chuev *et al.* [47] and Smith *et al.* [48] for H_3O^+ and Cl^- ions without additional modifications. The LJ parameters of σ_{ij} and ε_{ij} were determined according to the standard combining rules: $\sigma_{ij} = (\sigma_i + \sigma_j)/2$ and $\varepsilon_{ij} = \sqrt{\varepsilon_i \varepsilon_j}$. Because the H_3O^+ solvation energy ΔG_{solv} (H_3O^+) has a large contribution to the equilibrium potential of reaction (R1), the LJ parameters used for 1 M HCl aq. were tuned to reproduce the experimental value of $\Delta G_{solv}(H_3O^+) = 100$–$110$ kcal mol^{-1} (1 kcal = 4.184 kJ) [49]. An 1D-RISM calculation [50] of 1 M HCl aq., using the SPC model with modification to $\sigma_H = 1.0$ Å and $\varepsilon_H = 0.046$ kcal mol^{-1}, gave $\Delta G_{solv}(H_3O^+) = 80.8$ kcal mol^{-1}. Although this value is consistent with a previous RISM calculation with hypernetted chain closure [47], a significant underestimation of ΔG_{solv} was found. However, an 1D-RISM calculation using the TIP5P model with modifications of $\sigma_H = 1.0$ Å, $\sigma_L = 1.8$ Å, and $\varepsilon_H = \varepsilon_L = 0.046$ kcal mol^{-1} (L is lone pair) gave $\Delta G_{solv}(H_3O^+) = 102$ kcal mol^{-1}, which is in good agreement with the experiments. Therefore, we employed the TIP5P model for all of the ESM-RISM calculations in this study. The LJ parameters of the electrode atoms were $\sigma_{Pt} = 2.65$ Å, $\sigma_{Al} = 4.01$ Å, $\varepsilon_{Pt,Al} = 1.66$ kcal mol^{-1}, and $\varepsilon_{Al} = 0.505$ kcal mol^{-1}. The

LJ parameters of Pt were obtained by fitting the interaction energy between the Pt surface and Xe derived from van der Waals DFT calculations (the details will be discussed elsewhere), while those of Al were from the universal force field [51].

III. RESULTS

The grand potentials Ω of the left and right components in reaction (R1) on electrode M = Pt are expressed as

$$\Omega_{\rm L} = 1/2\{A({\rm H_2}, {\rm gas}) + E_{\rm ZP}({\rm H_2})\} + \Omega({\rm Pt_{36}} + {\rm H_2O}/1\,{\rm M\,HCl\,aq.}) + E_{\rm ZP}({\rm H_2O}), \quad (12a)$$

$$\Omega_{\rm R} = \Omega({\rm Pt_{36}} + {\rm H_3O^+}/1\,{\rm M\,HCl\,aq.}) + E_{\rm ZP}({\rm H_3O^+}), \quad (12b)$$

where $\Omega({\rm Pt_{36}} + {\rm H_2O}/1\,{\rm M\,HCl\,aq.})$ and $\Omega({\rm Pt_{36}} + {\rm H_3O^+}/1\,{\rm M\,HCl\,aq.})$ are the grand potentials calculated from Eq. (4) with the vacuum/slab+ion/solvent system in Fig. 2(c), $A({\rm H_2}, {\rm gas})$ is the sum of the DFT energy of an isolated H_2 molecule and the standard molar entropy term $-TS(= -298.15\,{\rm K}\times 130.6\,{\rm J\,mol^{-1}\,K^{-1}} = -0.404\,{\rm eV})$ [52] of H_2 gas, and $E_{\rm ZP}$ is the zero point vibrational energy of an isolated molecule or ion. These zero point energies were calculated by using the Gaussian16 program package with conditions of BLYP/6−311 + G(3df, 2pd): $E_{\rm ZP} = 0.270$, 0.562, and 0.909 eV for H_2, H_2O, and H_3O^+, respectively [53]. The ESM-RISM calculations were conducted at specific surface charge densities (e.g., $\sigma = \ldots, -0.4, -0.2, 0, 0.2, 0.4, \ldots e$/unit cell). The grand potentials $\Omega_{\rm L}$ and $\Omega_{\rm R}$ are shown as a function of $\mu_{\rm e}$ vs $\Phi_{\rm S}$ in Fig. 5(a).

For the system of $Pt_{36} + H_2O/1\,{\rm M\,HCl\,aq.}$, $\Omega_{\rm L}$ had an inverted parabola-shape centered at the point of $-\Delta N_{\rm e} = 0$, which is consistent with what is expected from a constant capacitance. $\mu_{\rm e} = -5.61$ eV at $\Delta N_{\rm e} = 0$ in this case was almost the same as $\mu_{\rm e}^{\rm PZC}({\rm Pt}) = -5.60$ eV obtained in Sec. II B, which indicated that the electric double layer screened the electronic interaction between the Pt surface and QM H_2O molecule sufficiently. Therefore, the curvature of the grand potential Ω consisted mainly of the double layer capacitance at the interface of Pt(111)/1 M HCl aq. In addition, the curvature of Ω with respect to $\mu_{\rm e}$ is related to the differential capacitance $C = -e^2/s(\partial^2\Omega/\partial{\mu_e}^2) = -e^2(\partial^2\gamma/\partial{\mu_e}^2)$, where s and γ are the surface area of the unit cell and the surface tension, respectively. The capacitance of Pt(111)/1 M HCl aq. was roughly estimated as 30–50 μF/cm^2, whose order was consistent with that of the PCM solvent [27] and a recently calculated value from DFT-MD simulations [54]. Since the force field parameters applied for ESM-RISM calculations could not express the specific adsorption of Cl^- ions, as has already been mentioned, the capacitance contribution from specific adsorptions was not included.

For the system of $Pt_{36} + H_3O^+/1\,{\rm M\,HCl\,aq.}$, the electric double layer on the Pt surface screened the interaction between the Pt(111) surface and the H_3O^+ ion in the solution, which led to $\mu_{\rm e} = -5.58\,{\rm eV} \approx \mu_{\rm e}^{\rm PZC}({\rm Pt})$ even at $-\Delta N_{\rm e} = +1$. $\Omega_{\rm R}$ showed an inverted parabola shape centered at $\mu_{\rm e} = -5.13$ eV at $\Delta N_{\rm e} = 0$. The crossing point of $\Omega_{\rm L}$ and $\Omega_{\rm R}$ showed that the state changed from H_3O^+(S) to H_2O(S) + 1/2H_2(gas) with increasing $\mu_{\rm e}$. Therefore, $\mu_{\rm e}$ at the crossing point was interpreted as the corresponding SHE potential: $\mu_{\rm e}^{\rm SHE} = -5.27$ eV. The electrode potential $E({\rm H^+/H_2})$ [vs $\Phi_{\rm S}$] was, then, obtained from Eq. (10). From Eq. (11), the chemical potentials of PZC and SHE gave the electrode potential at PZC $E_{\rm S}^{\rm M}(\sigma = 0) = -(\mu_{\rm e}^{\rm PZC} - \mu_{\rm e}^{\rm SHE})/e = 0.33$ V vs SHE, which was in good agreement with the experimental values of 0.36 [55] or 0.23 [56] V vs SHE. The electrode potential derived from $\mu_{\rm e}$ with the grand potential analysis came from the concept of the electrode potential from chemical potential, as discussed in Sec. II C.

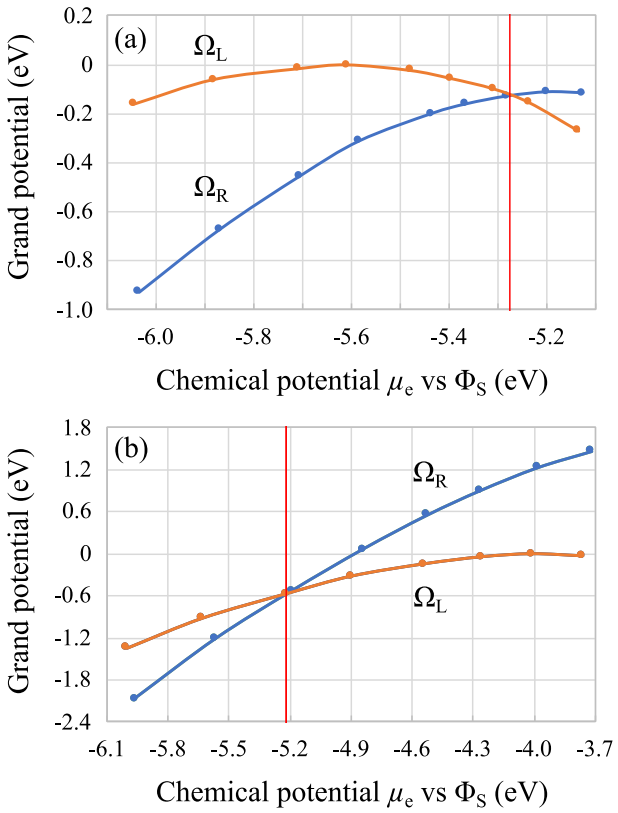

FIG. 5. Grand potentials $\Omega_{\rm L}$ (orange circles) and $\Omega_{\rm R}$ (blue circles) as a function of $\mu_{\rm e}$ vs $\Phi_{\rm S}$ at (a) Pt(111)/1 M HCl aq. and (b) Al(111)/1 M HCl aq. The orange and blue solid lines are provided as a guide for the eye. The origin of Ω is set at the value of $\Omega_{\rm L}$ at $\Delta N_{\rm e} = 0$. The red solid lines represent $\Delta G_{\rm SHE}$ derived from the vacuum/slab+ion/solvent system.

Another pathway for electrode potential from free energy difference could be applied. We can represent the free energy difference $\Delta G_{\rm SHE}$ in Eq. (9) as the free energy difference of the left and right sides of reaction (R1) at electrode M = Pt:

$$G_{\rm L} = 1/2\{A({\rm H_2}, {\rm gas}) + E_{\rm ZP}({\rm H_2})\} + A({\rm Pt_{36}} + {\rm H_2O}/1\,{\rm M\,HCl\,aq.}) + E_{\rm ZP}({\rm H_2O}), \quad (13a)$$

$$G_{\rm R} = A({\rm Pt_{36}} + {\rm H_3O^+}/1\,{\rm M\,HCl\,aq.}) + E_{\rm ZP}({\rm H_3O^+}), \quad (13b)$$

where $A({\rm Pt_{36}} + {\rm H_2O}/1\,{\rm M\,HCl\,aq.})$ and $A({\rm Pt_{36}} + {\rm H_3O^+}/1\,{\rm M\,HCl\,aq.})$ are the free energies calculated by ESM-RISM with the vacuum/slab+ion/solvent system shown in Fig. 2(c). The difference between Helmholtz free energy A and Gibbs free energy G, that is, volume × pressure contribution, was

not included in Eqs. (13). After the definition of G_L and G_R, $\Delta G_{SHE} = G_L - G_R = -5.27\,eV$ was obtained, which was the same value as μ_e^{SHE} from grand potential analysis [see the crossing point of Ω and the red solid line depicted in Fig. 5(a)]. Thus, the electrode potentials from chemical potential and from free energy difference gave the same value within the ESM-RISM treatment. It is emphasized that this equivalence is independent of the capacitance on the Pt(111)/1 M HCl aq., as shown in the Appendix. It should be mentioned that the grand potential analysis within ESM-RISM treatment could be applied for estimating the electrode potential associated with the "ion" adsorption reaction, such as OH^- in the case even including the effect of an electronic double layer, which will be discussed elsewhere.

It is possible to represent the free energy of the left and right sides of reaction (R1) without electrode M as

$$G'_L = 1/2\{A(H_2, gas) + E_{ZP}(H_2)\} + A(H_2O/1\,M\,HCl\,aq.) + E_{ZP}(H_2O), \quad (14a)$$

$$G'_R = A(H_3O^+/1\,M\,HCl\,aq.) + E_{ZP}(H_3O^+). \quad (14b)$$

$A(H_2O/1\,M\,HCl\,aq.)$ and $A(H_3O^+/1\,M\,HCl\,aq.)$ are calculated with the solvent/ion/solvent system shown in Fig. 2(d). ESM-RISM free energies in Eq. (5) gave $\Delta G'_{SHE} = G'_L - G'_R = -5.23\,eV$. The difference of 0.04 eV between ΔG_{SHE} and $\Delta G'_{SHE}$ might arise from the interactions between the Pt(111) surface and the ion and from the limitation of the QM ion interaction in the surface parallel direction. It is expected that a longer distance between the surface and QM ion and a larger surface area of the vacuum/slab+ion/solvent system will provide a convergence to the ideal value: $\Delta G_{SHE} \to \Delta G'_{SHE}$. Because the calculation cost of the solvent/ion/solvent system is negligible, compared with that of the vacuum/slab+ion/solvent system, the solvent/ion/solvent system is very useful when estimating interactions between a surface and an ion or between ions in the surface parallel direction.

The values of Ω_L and Ω_R after replacing the electrode of Pt with Al are shown in Fig. 5(b). At both the interfaces of $Al_{36} + H_2O/1\,M\,HCl\,aq.$ and $Al_{36} + H_3O^+/1\,M\,HCl\,aq.$, the grand potentials Ω_L and Ω_R had an inverted parabola shape centered at the point of $-\Delta N_e = 0$ as expected. The chemical potentials $\mu_e = -4.01$ and $-3.99\,eV$ at $-\Delta N_e = 0$ and $+1$ on the interfaces of $Al_{36} + H_2O/1\,M\,HCl\,aq.$ and $Al_{36} + H_3O^+/1\,M\,HCl\,aq.$, respectively, were close to μ_e^{PZC} (Al) $= -4.04\,eV$. The capacitance of Al(111)/1 M HCl aq. was roughly estimated as 10–20 $\mu F\,cm^{-2}$. The chemical potential of electrons derived at the crossing point of Ω_L and Ω_R was $\mu_e^{SHE} = -5.22\,eV$, which was almost equal to that of the Pt(111)/1 M HCl aq. From Eq. (11), the PZC of the Al(111) electrode gave $E_S^M(\sigma = 0) = -1.18\,V$ vs SHE. Since Al metal is experimentally dissolved or covered by oxidized Al in aqueous solutions, it is impossible to compare $E_S^M(\sigma = 0)$ with that obtained from experiments. The important point of the calculation with Al is that we could confirm the independency of the electrode potential on the electrodes.

IV. DISCUSSION

In this section we discuss the relation between the absolute SHE potential derived by Trasatti and the SHE potential vs Φ_S obtained in this study. From the schematic path for the calculation of the absolute SHE potential in Fig. 1, a previous reported value of $\Delta_S^M\psi = -1.1$ to $-1.4\,V$ from DFT-MD + ESM calculation [M = Pt(111)] [9], and the total potential v_{tot} on the Pt(111)/1 M HCl aq. system in Fig. 3(b), we can draw the potential energy profile through the vacuum/metal/solution/vacuum interface, as shown in Fig. 6. The potential deviation at the solution and vacuum interface is schematically depicted. The potential energy at a point in the left vacuum close to the surface of the electrode M is denoted as $\Phi_V \to \Phi_V^M$, to distinguish it from the potential energy at a point in the right vacuum close to the surface of the solution S, that is, the outer potential Φ_V^S of the solution. The difference between the inner and the outer potentials (the potential energy drop by a surface dipole) $-e\chi_S$, and the perturbation term arising from the double-layer polarization at metal-solution interface $-e\delta\chi_M$, are also indicated in Fig. 6. The relation among these two potentials and the contact potential difference ($\Delta_S^M\psi = \chi_S + \delta\chi_M$) has been discussed in the study with DFT-MD + ESM simulation by Otani *et al.* [9].

According to Trasatti, the absolute SHE potential $\mu_e^{SHE} = -4.44\,eV$ is measured from the outer potential Φ_V^S [7]. However, the Pt(111)/1 M HCl aq. system gave $\mu_e^{SHE} = -5.27\,eV$ referenced to the inner potential Φ_S. It is obvious that the difference between the inner and the outer potentials ($-e\chi_S$) needs to be compared: $E[abs] = E[vs\ \Phi_S] + \chi_S$. If we use the result of $\Delta_S^M\psi = -1.1$ to $-1.4\,V$ from the DFT-MD + ESM simulation [9], the calculation values of $\Phi_M = 5.77\,eV$ and $E_S^M(\sigma = 0) = 0.33\,V$ vs SHE on the Pt(111)/1 M HCl aq. yield $E(H^+/H_2)$ [abs] = 4.07 to 4.37 V from Eq. (3). Although this absolute SHE potential is a reasonable value compared with the experiment, the estimation of χ_S is very complicated because χ_S depends strongly on the pseudopotentials or effective force-field charges (see the air-water interface results by Kevin [57] and references therein). This fact indicates that Φ_S also depends on the force-field parameters. However, Φ_S is the possible reference as long as we use the same force-field parameters.

Trasatti suggested three conceivable reference levels for absolute potential [7]. One is an electron level in the ground state in a vacuum at "infinity." This infinity is not the point just outside the metal but far from the influence of the surface potential. The next and last references are the inner potential Φ_S and the outer potential Φ_V^S, which are adopted in ESM-RISM and by Trasatti, respectively. As already pointed out by Trasatti [7], Φ_S cannot be a universal reference state since it depends on the nature of the solution S. In fact, the energy of electrons at the Fermi level of the metal electrode M immersed in two different solvents is not necessarily the same. In addition, the experimental determination of the work function of a liquid polar phase presents more problems than that of a metal. Although the ESM-RISM calculation referenced to Φ_S makes it possible for a comparison between the electrode potentials at different electrodes immersed in the same solution, a method for the comparison between

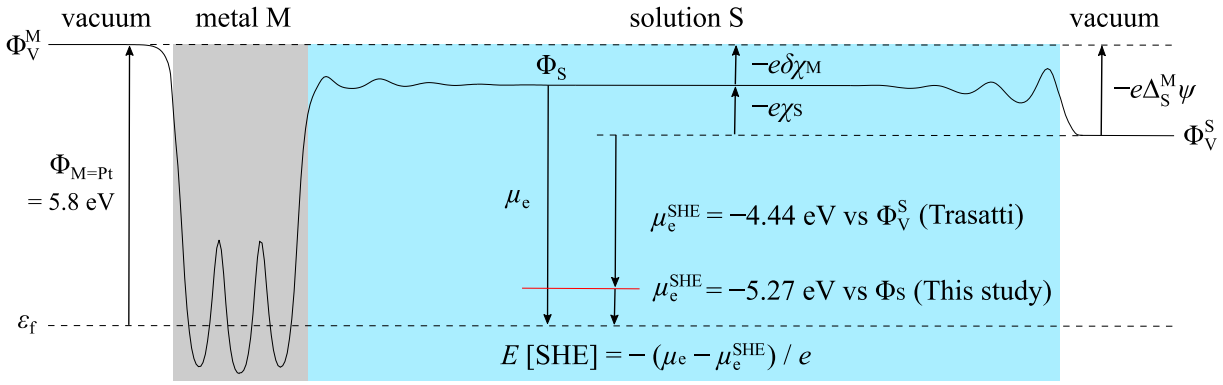

FIG. 6. Potential energy profile through the vacuum/metal/solution/vacuum interface.

the electrode potentials in different solutions remains to be determined in future studies.

V. CONCLUSIONS

We investigated the chemical potential of electrons corresponding to the SHE potential by employing DFT calculations combined with implicit solvation theory, referred to as ESM-RISM. In this calculation, the electrostatic field from the charged slab treated by DFT with ESM was completely screened out by that from the charge distribution of the electrolyte in the solution represented by RISM. This screening allowed us to define a reference potential, which was an inner potential Φ_S at the bulk solution region, and then the direct comparison of grand potentials and free energies between two different electrodes (but with the same solution) became possible. We compared the grand potentials Ω_L and Ω_R of two states for the charge transfer reaction (R1) with changing the chemical potential of electrons. The crossing point of Ω_L and Ω_R could be regarded as the corresponding SHE potential, which derived $\mu_e^{SHE} = -5.27$ eV vs Φ_S for the Pt(111) electrode. Another pathway from the free energy difference ΔG_{SHE} also indicated the same SHE potential, which validated the equivalence of electrode potentials from chemical potential and from free energy difference within the ESM-RISM treatment. As theoretically expected, a different electrode of Al gave almost the same value of $\mu_e^{SHE} = -5.22$ eV vs Φ_S. Thus, the electrode potential was confirmed to be independent of the electrodes. Finally, the relation between the absolute SHE potential and the Φ_S referred to the SHE potential was discussed. The schematic potential energy profile of a vacuum/metal/solution/vacuum interface indicated that the difference between the inner and the outer potentials is the origin of the difference between the two SHE values. This study establishes the concept of a well-defined electrode potential in computational electrochemistry.

ACKNOWLEDGMENTS

This work was supported by the R&D Initiative for scientific innovation of new generation batteries 2 Project (RISING2) administrated by the New Energy and Industrial Technology Department Organization (NEDO). This work was also supported in part by the MEXT projects of "Priority Issue on Post-K computer" (Development of new fundamental technologies for high-efficiency energy creation, conversion/storage and use) and JSPS KAKENHI Grant No. JP16K17969. The calculations were conducted on the K computer through the HPCI System Research Project (Project IDs: hp170117, hp180095) as well as the supercomputers in The University of Tokyo and Nagoya University.

APPENDIX

We consider the system of electrode M + ion A (or B). We assume that there is a sufficient distance between electrode M and ion A, thus the free energy and the number of electrons can be attributed to each part. The grand potential of the system M + A is represented as

$$\begin{aligned}\Omega(\mathrm{M+A}) &= F(\mathrm{M+A}) - \mu N_{\mathrm{M+A}} \\ &= F(\mathrm{M}) + F(\mathrm{A}) - \mu N_{\mathrm{M}} - \mu N_{\mathrm{A}}, \end{aligned} \quad \text{(A1)}$$

where the free energy $F(A)$ and the number of electrons N_A are independent of the chemical potential of the electrons μ. The same assumption is applied for the system of M + B:

$$\begin{aligned}\Omega(\mathrm{M+B}) &= F(\mathrm{M+B}) - \mu N_{\mathrm{M+B}} \\ &= F(\mathrm{M}) + F(\mathrm{B}) - \mu N_{\mathrm{M}} - \mu N_{\mathrm{B}}. \end{aligned} \quad \text{(A2)}$$

We obtain the chemical potential of electrons μ at the crossing point of Ω(M + A) and Ω(M + B), that is

$$\begin{aligned}&\Omega(\mathrm{M+A}) = \Omega(\mathrm{M+B}), \\ &F(\mathrm{M}) + F(\mathrm{A}) - \mu N_{\mathrm{M}} - \mu N_{\mathrm{A}} \\ &\quad = F(\mathrm{M}) + F(\mathrm{B}) - \mu N_{\mathrm{M}} - \mu N_{\mathrm{B}}, \\ &F(\mathrm{A}) - F(\mathrm{B}) = \mu(N_{\mathrm{A}} - N_{\mathrm{B}}), \\ &\mu = \frac{F(\mathrm{A}) - F(\mathrm{B})}{N_{\mathrm{A}} - N_{\mathrm{B}}}. \end{aligned} \quad \text{(A3)}$$

In Eq. (A3), $F(A) - F(B)$ can be interpreted as the free energy difference between ion A and B, and $N_A - N_B$ is the number of reacted electrons. Therefore, the chemical potential of electrons μ at the crossing point of Ω(M + A) and Ω(M + B) is equal to the free energy difference between ions A and B, which is independent of the capacitance at the electrode M.

[1] J. O'M. Bockris and A. K. N. Reddy, in *Modern Electrochemistry* (Plenum, New York, 1973).

[2] N. M. Marković and P. N. Ross Jr., Surf. Sci. Rep. **45**, 117 (2002).

[3] G. Girishkumar, B. McCloskey, A. C. Luntz, S. Swanson, and W. Wilcke, J. Phys. Chem. Lett. **1**, 2193 (2010); J.-S. Lee, S. T. Kim, R. Cao, N.-S. Choi, M. Liu, K. T. Lee, and J. Cho, Adv. Energy Mater. **1**, 34 (2011); G. G. Amatucci and N. Pereira, J. Fluorine Chem. **128**, 243 (2007).

[4] S. Trasatti, in *Advances in Electrochemistry and Electrochemical Engineering*, edited by H. Gerischer and C. W. Tobias (Wiley, New York, 1977), Vol. 10, p. 213.

[5] S. Trasatti, Electrochim. Acta **36**, 1659 (1991).

[6] R. Gomer and G. Tryson, J. Chem. Phys. **66**, 4413 (1977); E. R. Kötz, H. Neff, and K. Müller, J. Electroanal. Chem. Interfacial Electrochem. **215**, 331 (1986); W. N. Hansen and G. J. Hansen, Phys. Rev. A **36**, 1396 (1987); W. R. Fawcett, Langmuir **24**, 9868 (2008); A. A. Isse and A. Gennaro, J. Phys. Chem. B **114**, 7894 (2010).

[7] S. Trasatti, Pure Appl. Chem. **58**, 955 (1986).

[8] *IUPAC Compendium of Chemical Terminology*, 2nd ed. (the "Gold Book"). Compiled by A. D. McNaught and A. Wilkinson (Blackwell Scientific, Oxford, 1997).

[9] M. Otani, I. Hamada, O. Sugino, Y. Morikawa, Y. Okamoto, and T. Ikeshoji, J. Phys. Soc. Jpn. **77**, 024802 (2008).

[10] O. Sugino, I. Hamada, M. Otani, Y. Morikawa, T. Ikeshoji, and Y. Okamoto, Surf. Sci. **601**, 5237 (2007); M. Otani, I. Hamada, O. Sugino, Y. Morikawa, Y. Okamoto, and T. Ikeshoji, Phys. Chem. Chem. Phys. **10**, 3609 (2008); T. Ikeshoji, M. Otani, I. Hamada, and Y. Okamoto, *ibid.* **13**, 20223 (2011); T. Ikeshoji, M. Otani, I. Hamada, O. Sugino, Y. Morikawa, Y. Okamoto, Y. Qian, and I. Yagi, AIP Adv. **2**, 032182 (2012).

[11] V. Tripkovic, M. E. Björketun, E. Skúlason, and J. Rossmeisl, Phys. Rev. B **84**, 115452 (2011).

[12] S. Sakong, K. Forster-Tonigold, and A. Groß, J. Chem. Phys. **144**, 194701 (2016).

[13] J. Chen and M. Sprik, Phys. Rev. B **82**, 081406(R) (2010); Phys. Chem. Chem. Phys. **14**, 11245 (2012).

[14] J. Chen, M. Sulpizi, and M. Sprik, J. Chem. Phys. **131**, 154504 (2009); F. Costanzo, M. Sulpizi, R. G. D. Valle, and M. Sprik, *ibid.* **134**, 244508 (2011); J. Cheng, X. Liu, J. VandeVondele, M. Sulpizi, and M. Sprik, Acc. Chem. Res. **47**, 3522 (2014).

[15] J. Le, M. Iannuzzi, A. Cuesta, and J. Chen, Phys. Rev. Lett. **119**, 016801 (2017).

[16] J. K. Nørskov, J. Rossmeisl, A. Logadottir, L. Lindqvist, J. R. Kitchin, T. Bligaard, and H. Jónsson, J. Phys. Chem. B **108**, 17886 (2004); J. K. Nørskov, T. Bligaard, J. Rossmeisl, and C. H. Christensen, Nat. Chem. **1**, 37 (2009).

[17] J. K. Nørskov, T. Bligaard, A. Logadottir, J. R. Kitchin, J. G. Chen, S. Pandelov, and U. Stimming, J. Electrochem. Soc. **152**, J23 (2005).

[18] G. S. Karlberg, J. Rossmeisl, and J. K. Nørskov, Phys. Chem. Chem. Phys. **9**, 5158 (2007).

[19] H. A. Hansen, J. Rossmeisl, and J. K. Nørskov, Phys. Chem. Chem. Phys. **10**, 3722 (2008).

[20] K. Chan and J. K. Nørskov, J. Phys. Chem. Lett. **6**, 2663 (2015).

[21] T. Ikeshoji and M. Otani, Phys. Chem. Chem. Phys. **19**, 4447 (2017); T. Ikeshoji, T. Uchida, M. Otani, and M. Osawa, J. Electroanal. Chem. **800**, 13 (2017).

[22] J. Haruyama, T. Ikeshoji, and M. Otani, J. Phys. Chem. C **122**, 9804 (2018).

[23] J.-S Filhol and M. Neurock, Angew. Chem. Int. Ed. **45**, 402 (2006); C. D. Taylor, S. A. Wasileski, J.-S Filhol, and M. Neurock, Phys. Rev. B **73**, 165402 (2006); S. Schnur and A. Groß, Catalysis Today **165**, 129 (2011).

[24] R. Jinnouchi and A. B. Anderson, Phys. Rev. B **77**, 245417 (2008); J. Phys. Chem. C **112**, 8747 (2008); R. Jinnouchi, K. Kodama, T. Suzuki, and Y. Morimoto, J. Chem. Phys. **142**, 184709 (2015).

[25] S. A. Petrosyan, A. A. Rigos, and T. A. Arias, J. Phys. Chem. B **109**, 15436 (2005); K. Letchworth-Weaver and T. A. Arias, Phys. Rev. B **86**, 075140 (2012).

[26] O. Andreussi, I. Dabo, and N. Marzari, J. Chem. Phys. **136**, 064102 (2012).

[27] N. Lespes and J.-S. Filhol, J. Chem. Theory Comput. **11**, 3375 (2015).

[28] S. Woelki, H.-H Kohler, and H. Krienke, J. Phys. Chem. B **111**, 13386 (2007); **112**, 3365 (2008).

[29] N. B. Luque, S. Woelki, D. Henderson, and W. Schmickler, Electrochim. Acta **56**, 7298 (2011).

[30] R. G. Parr and W. T. Yang, *Density Functional Theory of Atoms and Molecules* (Oxford University Press, New York, 1989).

[31] A. Y. Lozovoi, A. Alavi, J. Kohanoff, and R. M. Lynden-Bell, J. Chem. Phys. **115**, 1661 (2001).

[32] N. Bonnet, T. Morishita, O. Sugino, and M. Otani, Phys. Rev. Lett. **109**, 266101 (2012).

[33] P. Hohenberg and W. Kohn, Phys. Rev. **136**, B864 (1964); W. Kohn and L. J. Sham, *ibid.* **140**, A1133 (1965).

[34] A. Kovalenko and F. Hirata, J. Chem. Phys. **110**, 10095 (1999).

[35] M. Otani and O. Sugino, Phys. Rev. B **73**, 115407 (2006).

[36] S. Nishihara and M. Otani, Phys. Rev. B **96**, 115429 (2017).

[37] G. Hummer, L. R. Pratt, and A. E. García, J. Phys. Chem. **100**, 1206 (1996); K. Leung, S. B. Rempe, and O. A. von Lilienfeld, J. Chem. Phys. **130**, 204507 (2009); K. Leung and C. M. Tenney, J. Phys. Chem. C **117**, 24224 (2013).

[38] J. Haruyama, K. Sodeyama, L. Han, K. Takada, and Y. Tateyama, Chem. Mater. **26**, 4248 (2014); J. Haruyama, K. Sodeyama, and Y. Tateyama, ACS Appl. Mater. Interfaces **9**, 286 (2017).

[39] P. Giannozzi *et al.*, J. Phys.: Condens. Matter **21**, 395502 (2009); **29**, 465901 (2017).

[40] J. P. Perdew, K. Burke, and M. Ernzerhof, Phys. Rev. Lett. **77**, 3865 (1996); **78**, 1396 (1997).

[41] D. Vanderbilt, Phys. Rev. B **41**, 7892 (1990); A. M. Rappe, K. M. Rabe, E. Kaxiras, and J. Joannopoulos, *ibid.* **41**, 1227 (1990).

[42] S. G. Louie, S. Froyen, and M. L. Cohen, Phys. Rev. B **26**, 1738 (1982).

[43] K. Momma and F. Izumi, J. Appl. Crystallogr. **44**, 1272 (2011).

[44] D. Chandler, Y. Singh, and D. M. Richardson, J. Chem. Phys. **81**, 1975 (1984).

[45] H. J. C. Berendsen, J. P. M. Postma, W. F. von Gunstaren, and J. Hermans, in *Intermolecular Forces*, edited by B. Pullman (Reidel, Dordrecht, Holland, 1981), p. 331.

[46] M. W. Mahoney and W. L. Jorgensen, J. Chem. Phys. **112**, 8910 (2000).

[47] G. N. Chuev, S. Chiodo, S. E. Erofeeva, M. V. Fedorov, N. Russo, and E. Sicilia, Chem. Phys. Lett. **418**, 485 (2006).

[48] D. E. Smith and L. X. Dang, J. Chem. Phys. **100**, 3757 (1994).
[49] R. G. Pearson, J. Am. Chem. Soc. **108**, 6109 (1986); J. Florián and A. Warshel, J. Phys. Chem. B **101**, 5583 (1997); J. R. Pliego Jr. and J. M. Riveros, Phys. Chem. Chem. Phys. **4**, 1622 (2002).
[50] F. Hirata and P. J. Rossky, Chem. Phys. Lett. **83**, 329 (1981).
[51] A. K. Rappe, C. J. Casewit, K. S. Colwell, W. A. Goddard III, and W. M. Skiff, J. Am. Chem. Soc. **114**, 10024 (1992).
[52] http://www2.ucdsb.on.ca/tiss/stretton/database/inorganic_thermo.htm
[53] M. J. Frisch *et al.*, Gaussian 16, Revision B.01, Gaussian, Inc., Wallingford CT, 2016; NIST Computational Chemistry Comparison and Benchmark Database NIST Standard Reference Database, 2018, edited by Russell D. Johnson III.
[54] A. Bouzid and A. Pasquarello, J. Phys. Chem. Lett. **9**, 1880 (2018).
[55] T. Pajkossy and D. M. Kolb, Electrochim. Acta **46**, 3063 (2001).
[56] A. Cuesta, Surf. Sci. **572**, 11 (2004).
[57] K. Leung, J. Phys. Chem. Lett. **1**, 496 (2010).